JOURNAL OF SOLID STATE CHEMISTRY **124,** 287–291 (1996)
ARTICLE NO. 0238

Preparation of a New Triclinic Phase Based on a Pseudo-fcc Subcell in the Systems Bi_2O_3–Ln_2O_3 (*Ln* = Dy, Ho, Er, and Y)

Akiteru Watanabe

National Institute for Research in Inorganic Materials, 1-1 Namiki, Tsukuba, Ibaraki 305, Japan

Received November 13, 1995; in revised form February 26, 1996; accepted April 4, 1996

A phase equilibrium study of the systems Bi_2O_3–Ln_2O_3 (*Ln* = lanthanoid including Y) has found a new phase, $Bi_{1-x}Ln_xO_{1.5}$ (*Ln* = Dy, Ho, Er, and Y with x = 0.485, 0.485–0.49, 0.49, and 0.475–0.49, respectively). A repetitive long-term solid-state reaction at about 800°C has generated this low-temperature stable phase. It crystallizes in the triclinic system with $a \simeq 8.5$ Å, $b \simeq 10$ Å, $c \simeq 8.5$ Å, $\alpha \simeq 111°$, $\beta \simeq 106°$, $\gamma \simeq 94°$, and $Z = 16$. This triclinic structure is based on a pseudo-fcc subcell with $a' \simeq 5.4$ Å. The axial relations between the triclinic supercell and the subcell are $a \simeq \sqrt{5}/2a'$, $b \simeq \sqrt{7}/2a'$, and $c \simeq \sqrt{5}/2a'$. When heated, the triclinic phase transforms smoothly into the δ-Bi_2O_3 type high-temperature stable phase around 1000°C; when it is cooled, its rate of transition in the opposite direction is extremely sluggish. This sluggishness seems to be due to the ordering of the cations, Bi^{3+} and Ln^{3+}, in the triclinic structure.

INTRODUCTION

The stabilization of the high-temperature polymorph of bismuth sesquioxide (δ-Bi_2O_3) with an oxide additive has been extensively studied from the viewpoint of realizing a low-temperature high-oxide-ion conductor, because δ-Bi_2O_3, stable between 730 and 825°C (1–3), is characterized by excellent oxide-ion conductivity (4, 5). Results have shown that a lanthanoid oxide (Ln_2O_3 including Y_2O_3) is effective in stabilizing the δ phase at low temperatures. Thus, in particular, the Er_2O_3-doped δ phase and the Y_2O_3-doped phase have been intensively investigated (5–18).

Phase equilibrium studies of the Bi-rich sides of the systems Bi_2O_3–Ln_2O_3 have revealed the existence of two low-temperature stable phases. One phase appears around 22.5 mol% Ln_2O_3 (*Ln* = La–Er and Y), forms a solid solution having a hexagonal layered structure with space group $R\bar{3}m$, $a \simeq 4$ Å, $c \simeq 24$ Å, $Z = 9$ ($Bi_{1-x}Ln_xO_{1.5}$) (19–22), and transforms into the high-temperature stable δ phase upon being heated, at around 670–900°C depending on *Ln* (19–22). The other low-temperature phase exists around 35 mol% Ln_2O_3 (*Ln* = Sm–Dy and Y) with a narrow solid solution extension, has a C-type rare-earth oxide-related structure crystallizing in the space group $I2_13$ with $a \simeq 11$ Å and $Z = 32$($Bi_{1-x}Ln_xO_{1.5}$) (23–25), and changes into the high-temperature stable δ phase upon being heated, at about 900°C (23–25). The existence of these low-temperature stable phases indicates that in these systems the Ln_2O_3-stabilized δ phase described so far is nothing but the quenched high-temperature phase and is metastable at temperatures lower than the transition temperature under thermodynamic equilibrium conditions. These results induced us to reexamine the phase equilibrium of the systems Bi_2O_3–Ln_2O_3 over the *Ln*-rich compositional region. As a result, a triclinic novel low-temperature stable phase based on a pseudo-fcc subcell has been found at around 48.5 mol% Ln_2O_3 in the systems with *Ln* = Dy–Er and Y.

EXPERIMENTAL PROCEDURE

Polycrystalline samples of $Bi_{1-x}Ln_xO_{1.5}$ (x = 0.2–0.6) were prepared by solid-state reaction of Bi_2O_3 (99.9%, Iwaki Chemicals Ltd.) and Ln_2O_3 (*Ln* = Dy, Ho, Er, and Y; 99.9%, Shin-Etsu Chemical Co., Ltd.). All the lanthanoid oxides were prefired at 600–700°C in air for dehydration before being used. The desired proportions were accurately weighed and thoroughly mixed with ethanol in an agate mortar. After being dried naturally in the room, the mixture was transferred into a covered platinum crucible and heated at about 800°C for about 150 hr or more. The product was then quenched to room temperature by an airstream. The same heat treatment was repeated several times after intermediate grindings to complete the reaction. All samples were examined after every quenching process by X-ray powder diffraction (XRPD) using Cu$K\alpha$ radiation and a diffracted-beam monochromator.

Since the repetitive long-term heat treatment might induce compositional change by ignition loss, the composition of the new phase was checked by chemical analysis using chelatometric titration with EDTA and xylenol orange indicator. A sample with the nominal composition $Bi_{0.51}Y_{0.49}O_{1.5}$ was chosen as representative, because this sample underwent heat treatment three times (at 806°C

0022-4596/96 $18.00

for 138 hr, at 809°C for 183 hr, and at 808°C for 350 hr) to turn the starting powder mixture completely into the pure new phase. The result was 51.06 ± 0.01 mol% Bi_2O_3 and 48.94 ± 0.01 mol% Y_2O_3. The compositional change is negligible. That is, the actual composition is virtually equal to the nominal one. At the same time, we checked the platinum contamination from the crucible using the ICP method on the same sample. The results showed that the contamination was negligible (<100 ppm).

In order to check preliminary lattice parameters and the crystal system, Visser's indexing program (26) was applied to the observed XRPD data measured with the continuous scanning method at a scanning rate of 0.4° min^{-1}. The 2θ values were corrected using the external standard of a Si powder. Moreover, using these results, the precise lattice parameters were calculated by the least-squares method (27).

The thermal behavior was checked by differential thermal analysis (DTA). About 100 mg of powder sample underwent heating–cooling cycles at a rate of 10°C min^{-1} in air to the maximum temperature of 1200°C. The reference material was α-Al_2O_3.

The density of the powder sample was measured using a gas pycnometer (Micromeritics Accupyc 1330). The sample weight was about 20 g.

RESULTS AND DISCUSSION

Figure 1 presents a series of XRPD patterns for $Bi_{0.515}Dy_{0.485}O_{1.5}$ typical of a sluggish solid-state reaction. Each pattern was taken just after the sequent heat treatment under the conditions inserted. The first heat treatment (Fig. 1a) produces a mixture of a Dy_2O_3-doped δ phase and a Dy-rich neighboring phase with a LaOF-type structure (28); the reflections based on the δ phase (fcc with $a \simeq 5.4$ Å) are indicated by solid circles. The second heating (Fig. 1b) leads to the unknown phase with appreciable intensities, while the reflections based on both phases mentioned above tend to be weakened explicitly. Clearly, the presence of three phases indicates that the system does not reach its equilibrium state under the present conditions because of the sluggish solid-state reaction. The third heat treatment (Fig. 1c) generates a major part of the unknown phase, and the fourth heating completely results in the pure unknown new phase (Fig. 1d).

The indexing result of the computer program showed that this phase crystallizes in the triclinic system. Figure 2 presents the indexed XRPD pattern of $Bi_{0.52}Y_{0.48}O_{1.5}$. The isomorphous new triclinic phase was identified as having the following composition in each system investigated: 48.5 mol% Dy_2O_3, 48.5–49 mol% Ho_2O_3, 49 mol% Er_2O_3, and 47.5–49 mol% Y_2O_3. Above and below these compositional ranges, two-phase regions appeared. Above the ranges, a second phase was the *Ln*-rich neighboring phase

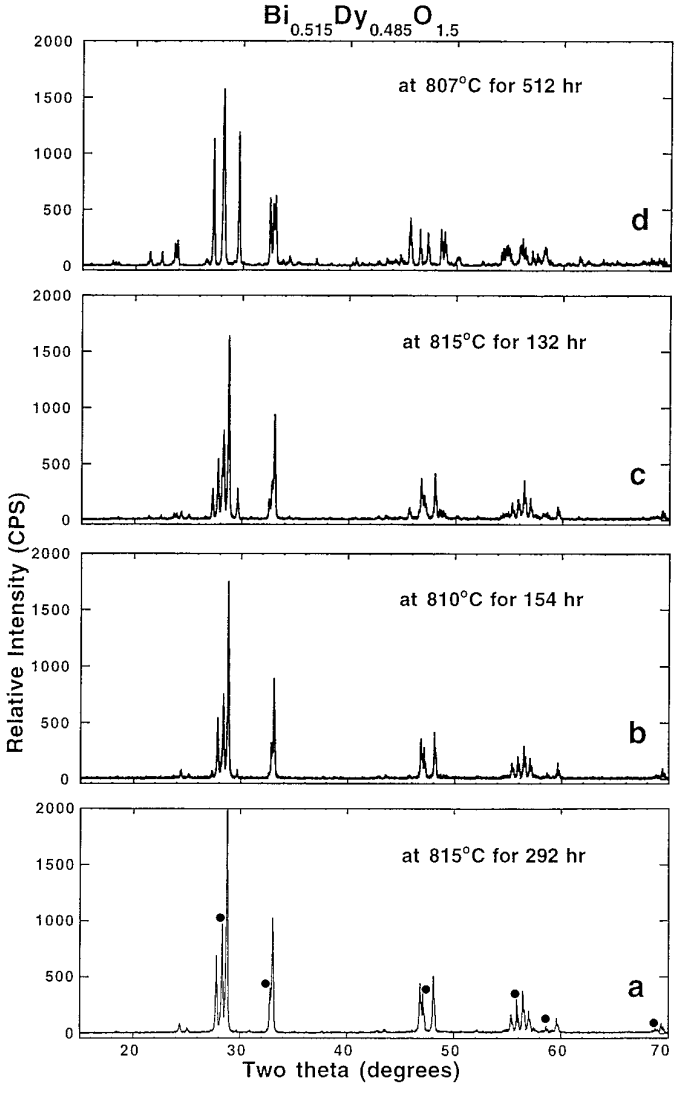

FIG. 1. The room-temperature XRPD patterns of $Bi_{0.515}Dy_{0.485}O_{1.5}$ using Cu$K\alpha$ radiation after heat treatment under the indicated conditions of temperature(°C)/time(hr). The fcc reflections designated by solid circles in (a) belong to a Dy_2O_3-doped δ phase and the other reflections to a LaOF-type phase.

with LaOF-type structure as shown in Fig. 1a. Needless to say, the same two-phase mixture was observed in the equimolar composition ($x = 0.5$). By contrast, below the ranges, the second phase depends on *Ln*: a bcc phase (23–25) in the case of *Ln* = Dy and Y, and a hexagonal phase (19–22) in the case of *Ln* = Ho and Er. The precise lattice parameters and both theoretical and measured densities are tabulated in Table 1 for the representative composition in each system. It is noted that the ionic radius of Y^{3+} is approximately equal to that of Ho^{3+} as reported by Shannon (29); i.e., $r(Y^{3+}) = 0.900$ Å and $r(Ho^{3+}) = 0.901$ Å. Table 2 gives the observed and calculated d values and relative intensities of XRPD lines with $I_{obs} \geqq 2$ for

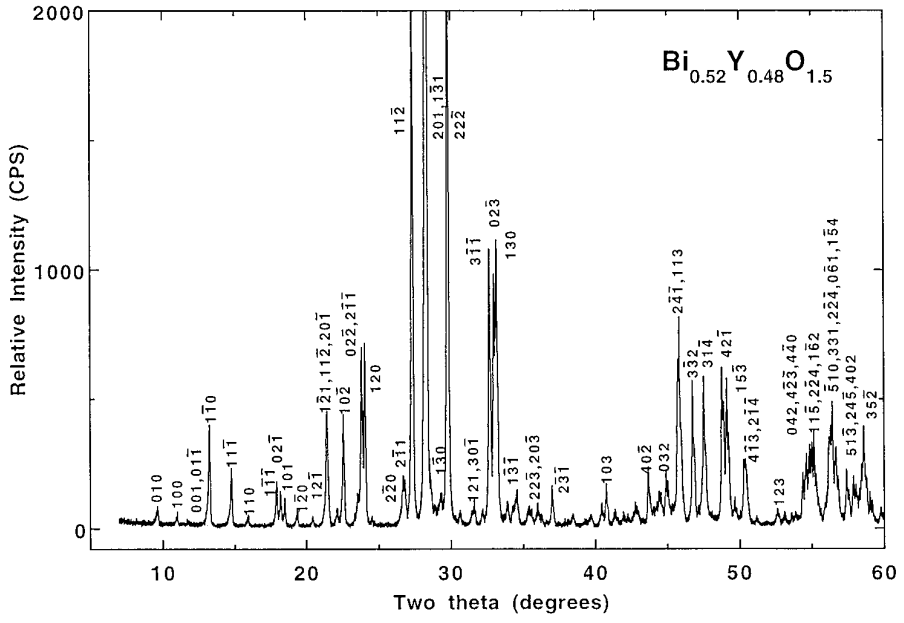

FIG. 2. The indexed XRPD pattern of a new triclinic phase with $Bi_{0.52}Y_{0.48}O_{1.5}$.

$Bi_{0.51}Er_{0.49}O_{1.5}$ along with Miller indices of a pseudo-fcc lattice which is ascribable to the fundamental reflections; we discuss this structural aspect later.

Figure 3 shows a typical DTA trace for the present triclinic phase of $Bi_{0.515}Ho_{0.485}O_{1.5}$: a widespread endothermic peak is detected around 1000°C only in the first heating direction. The same thermal behavior was observed for each of the other systems. The onset temperature of the broad endothermic peak was adopted as an approximate transition temperature. The transition temperature of the representative composition in each system was as follows: ca. 980°C for $Bi_{0.515}Dy_{0.485}O_{1.5}$, ca. 995°C for $Bi_{0.515}Ho_{0.485}O_{1.5}$, ca. 995°C for $Bi_{0.51}Er_{0.49}O_{1.5}$, and ca. 1010°C

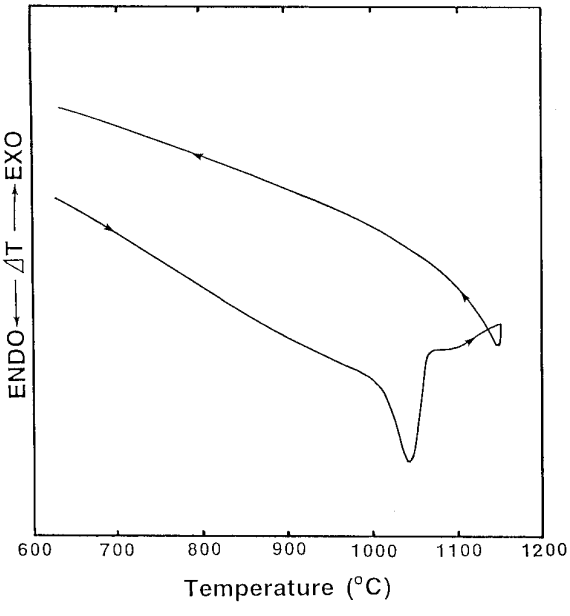

FIG. 3. DTA curve in the heating and cooling cycle for $Bi_{0.515}Ho_{0.485}O_{1.5}$.

TABLE 1
Lattice Parameters and Theoretical and Measured Densities of $Bi_{1-x}Ln_xO_{1.5}$

Ln	*x*	*a*(Å) *α*(°)	*b*(Å) *β*(°)	*c*(Å) *γ*(°)	*V*(Å^3) d_{calc}(g · cm^{-3}) d_{meas}(g · cm^{-3})
Dy	0.485	8.539(0)	10.056(1)	8.604(0)	650.1(0)
		111.45(0)	105.90(1)	93.65(1)	8.599
					8.592(2)
Ho	0.485	8.510(0)	10.018(1)	8.575(0)	643.6(0)
		111.36(0)	105.88(0)	93.77(1)	8.734
					8.720(7)
Ho	0.490	8.507(1)	10.014(1)	8.572(1)	642.9(1)
		111.36(1)	105.88(1)	93.76(1)	8.736
Er	0.490	8.475(1)	9.982(1)	8.541(1)	636.3(1)
		111.30(0)	105.83(1)	93.86(1)	8.874
					8.846(4)
Y	0.475	8.507(0)	10.017(1)	8.572(1)	643.2(0)
		111.34(0)	105.88(1)	93.77(1)	7.266
Y	0.480	8.504(1)	10.015(1)	8.570(1)	642.7(1)
		111.34(0)	105.87(1)	93.76(1)	7.248
					7.227(3)
Y	0.490	8.504(0)	10.013(1)	8.569(0)	642.5(0)
		111.35(0)	105.86(0)	93.76(1)	7.200

TABLE 2
X-Ray Powder Diffraction Data for $Bi_{0.51}Er_{0.49}O_{1.5}$

h	k	l	d_{calc} (Å)	d_{obs} (Å)	I_{obs}[a]	h'	k'	l'[b]
0	1	0	9.137	9.140	2			
1	0	0	8.011	8.015	2			
1	0	−1	6.654	6.651	3			
1	1	−1	5.966	5.962	4			
2	0	−1	4.126	4.126	5			
1	1	−2	4.126					
1	0	−2	3.929	3.927	6			
0	0	2	3.769	3.766	2			
0	2	−2	3.724	3.722	10			
2	−1	−1	3.724					
1	2	0	3.684	3.683	11			
2	−2	0	3.334	3.334	2			
2	0	−2	3.327	3.326	2			
2	−1	1	3.308	3.308	2			
1	−1	−2	3.248	3.247	63	1	1	−1
2	0	1	3.144	3.143	89	1	−1	1
1	−3	1	3.135	3.137	100	1	−1	−1
2	2	−1	3.103	3.101	3			
1	−3	0	3.040	3.040	2			
0	3	−2	3.030	3.033	2			
2	2	−2	2.9833	2.9819	66	1	1	1
3	−1	−1	2.7284	2.7272	33	2	0	0
0	2	−3	2.7019	2.7015	31	0	2	0
1	3	0	2.6860	2.6852	32	0	0	2
1	0	−3	2.6523	2.6524	2			
2	−3	1	2.6371	2.6378	2			
2	1	−3	2.6297	2.6312	2			
1	1	2	2.6055	2.6063	2			
1	−2	−2	2.5931	2.5928	5			
1	−3	−1	2.5839	2.5859	4			
2	2	−3	2.5315	2.5315	2			
2	0	−3	2.5229	2.5238	2			
2	−3	−1	2.4204	2.4202	3			
3	−3	0	2.2232	2.2233	2			
1	0	3	2.2047	2.2050	3			
1	1	−4	2.1054	2.1052	2			
1	4	0	2.0964	2.0967	2			
4	0	−2	2.0632	2.0639	4			
2	−3	−2	2.0544	2.0567	2			
4	−1	0	2.0371	2.0374	2			
2	−2	3	2.0304	2.0308	3			
4	1	−2	2.0239	2.0242	2			
0	3	2	2.0102	2.0106	5			
0	3	−4	1.9970	1.9972	2			
3	3	−3	1.9889	1.9889	2			
2	−4	−1	1.9767	1.9770	15	2	0	−2
1	1	3	1.9709	1.9712	21	0	−2	2
3	−3	2	1.9353	1.9356	17	2	−2	0
3	−4	0	1.9212	1.9214	2			
3	0	2	1.9097	1.9095	3			
3	1	−4	1.9047	1.9047	16	2	2	0
4	2	−1	1.8571	1.8573	17	2	0	2
1	5	−3	1.8450	1.8451	17	0	2	2
1	3	2	1.8274	1.8268	2			
4	−1	−3	1.8053	1.8052	5			

[a] Weak reflections (<2) are omitted to reduce the table.
[b] Miller indices based on the pseudo-fcc subcell.

for $Bi_{0.52}Y_{0.48}O_{1.5}$. No thermal effect on the traces through the subsequent cooling process and the second heating–cooling run was observed. An XRPD pattern of each sample after DTA measurement exhibited the fcc lattice, viz., the doped δ phase. The result indicates that the low-temperature stable triclinic phase transforms irreversibly into the high-temperature stable, doped δ phase. As evident from Fig. 1 and the following stability examination, however, this irreversibility is only apparent. In fact, the rate of transition from the δ to the triclinic phase is extremely sluggish in contrast to that of the opposite direction from the triclinic to the δ phase; that is, this transition is essentially reversible. In order to prepare the pure triclinic phase, therefore, the samples were heated at about 800°C (e.g., 807–815°C in Fig. 1), much lower than the transition temperatures, for a longer period (e.g., 132–512 hr in Fig. 1).

The thermal stability of the triclinic phase was checked in the following way for the representative specimen $Bi_{0.515}Ho_{0.485}O_{1.5}$. A quenched, doped δ phase prepared beforehand by solid-state reaction at 1150°C for 15 hr was annealed at about 800°C for 250 hr. After being annealed, the sample was quenched, then ground well in an agate mortar, and checked by XRPD. A similar annealing treatment was repeated five times. As a result, the doped δ phase transformed perfectly into the triclinic phase. That is, since the triclinic phase was generated not only by heating at temperatures lower than the polymorphic transition temperature but also by transformation from the high-temperature stable δ phase, it was clearly proved that the triclinic phase is the truly low-temperature stable phase. At the same time, it is noted that the doped δ phase was generated even at temperatures (Fig. 1) lower than the transition temperature around 950°C. These results indicate that the present phases obey the Ostwald step rule in the same way as the phases with C-type rare-earth oxide-related structure in the systems Bi_2O_3–Ln_2O_3 (Ln = Sm–Dy and Y) (24, 25). Thus, the doped δ phase is first formed over a wide temperature range and cooled easily to room temperature in the metastable state, so that the present triclinic phase has never been found to date.

Density was measured for the following typical composition in each system: $Bi_{0.515}Dy_{0.485}O_{1.5}$, $Bi_{0.515}Ho_{0.485}O_{1.5}$, $Bi_{0.51}Er_{0.49}O_{1.5}$, and $Bi_{0.52}Y_{0.48}O_{1.5}$. The results are listed in Table 1. From these density values and the lattice parameters listed in Table 1, it is clear that the unit cell of the triclinic phase contains 16 formula weights, $Z = 16(Bi_{1-x}Ln_xO_{1.5})$, where Ln = Dy–Er and Y.

The XRPD patterns shown in Figs. 1 and 2 suggest that the triclinic phase is connected to the δ phase in which the Bi and Ln atoms occupy their sites randomly; in other words, the triclinic phase forms a supercell based on a pseudo-fcc subcell closely related to the δ phase. The fundamental reflections on the subcell are labeled h' k' l' in

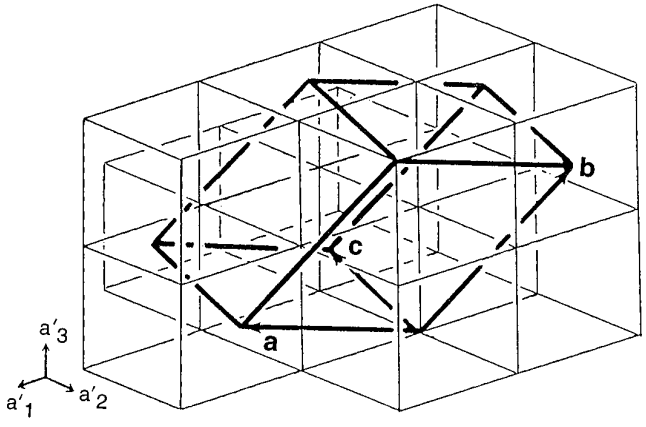

FIG. 4. Schematic representation of the relations of the unit-cell axes. Heavy solid lines show the triclinic cell (a, b, c) and weak solid lines outline the pseudo-fcc subcells (a'). Cations might occur at about all pseudo-cube corners and face centers.

Table 2. Thus, examination of the triclinic indices $h\ k\ l$ corresponding to these $h'\ k'\ l'$ indicated the topotactic relationship between the triclinic and pseudo-fcc lattices. That is, the transformation matrix for the direct-lattice unit-cell vectors from the pseudo-fcc lattice ($a' \simeq 5.4$ Å) to the triclinic lattice (a, b, c) is (3/2, 0, 1/2)/(−1/2, 1, 3/2)/(−1/2, −3/2, 0). Figure 4 exhibits these topotactic relations: $a \simeq \sqrt{5}/2a'$, $b \simeq \sqrt{7}/2a'$, and $c \simeq \sqrt{5}/2a'$. The value of the determinant of the transformation, 4, means that the triclinic cell is four times the size of the pseudo-fcc subcell. Since the fcc cell contains four lattice points, there are $4 \times 4 = 16$ lattice points in the triclinic cell. This result is in good agreement with $Z = 16(Bi_{1-x}Ln_xO_{1.5})$, determined from the measured density and the lattice volume listed in Table 1. Thus, the appearance of the triclinic phase might be due to the ordering of Bi and Ln atoms in the pseudo-fcc cation sublattice in the same way as in the Bi-rich neighboring phase with a C-type rare-earth oxide-related structure (24).

Although single crystal X-ray diffraction analysis is strictly necessary for structure determination, single crystal preparation is very difficult, because the liquidus temperatures are too high, probably >1500°C (25), to suppress the decomposition and because, if possible, the primary phase from the melt is the doped δ phase, not the present triclinic phase. To obtain the single crystal, for this reason, some special technique such as a flux method or a hydrothermal method might have to be employed. Therefore, an outline of the structure is under investigation using only the XRPD data.

ACKNOWLEDGMENTS

The author thanks Mr. S. Takenouchi and Mr. Y. Yajima for checking the sample composition by chemical analysis.

REFERENCES

1. E. M. Levin and R. S. Roth, *J. Res. Nat. Bur. Stand. Sect. A* **68,** 189 (1964).
2. H. A. Harwig and A. G. Gerards, *Thermochim. Acta* **28,** 121 (1979).
3. H. A. Harwig, *Z. Anorg. Allg. Chem.* **444,** 151 (1978).
4. M. G. Hapase and V. B. Tare, *Indian J. Pure Appl. Phys.* **5,** 401 (1967).
5. T. Takahashi, H. Iwahara, and T. Arao, *J. Appl. Electrochem.* **5,** 187 (1975).
6. M. J. Verkerk, K. Keizer, and A. J. Burggraaf, *J. Appl. Electrochem.* **10,** 81 (1980).
7. M. J. Verkerk and A. J. Burggraaf, *Solid State Ionics* **3/4,** 463 (1981).
8. A. J. Burggraaf, T. van Dijk, and M. J. Verkerk, *Solid State Ionics* **5,** 519 (1981).
9. M. J. Verkerk, G. M. H. van de Velde, A. J. Burggraaf, and R. B. Helmholdt, *J. Phys. Chem. Solids* **43,** 1129 (1982).
10. W. N. Lawless and S. L. Swartz, *Phys. Rev. B* **28,** 2125 (1983).
11. C. Wang, X. Xu, and B. Li, *Solid State Ionics* **13,** 135 (1984).
12. P. Duran, J. R. Jurado, C. Moure, N. Valverde, and B. C. H. Steele, *Mater. Chem. Phys.* **18,** 287 (1987).
13. H. Kruidhof, K. Seshan, B. C. Lippens Jr., P. J. Gellings, and A. J. Burggraaf, *Mater. Res. Bull.* **22,** 1635 (1987).
14. H. Kruidhof, K. Seshan, G. M. H. van de Velde, K. J. de Vries, and A. J. Burggraaf, *Mater. Res. Bull.* **23,** 371 (1988).
15. H. Kruidhof, K. J. de Vries, and A. J. Burggraaf, *Solid State Ionics* **37,** 213 (1990).
16. A. V. Joshi, S. Kulkarni, J. Nachlas, J. Diamond, N. Weber, and A. V. Virkar, *J. Mater. Sci.* **25,** 1237 (1990).
17. H. Kruidhof, H. J. M. Bouwmeester, K. J. de Vries, P. J. Gellings, and A. J. Burggraaf, *Solid State Ionics* **50,** 181 (1992).
18. K. Huang, C. Wang, and X. Xu, *J. Solid State Chem.* **98,** 206 (1992).
19. A. Watanabe and T. Kikuchi, *Solid State Ionics* **21,** 287 (1986).
20. A. Watanabe, *Solid State Ionics* **34,** 35 (1989).
21. P. Conflant, C. Follet-Houttemane, and M. Drache, *J. Mater. Chem.* **1,** 649 (1991).
22. A. Watanabe, M. Drache, J. P. Wignacourt, P. Conflant, and J. C. Boivin, *Solid State Ionics* **67,** 25 (1993).
23. A. Watanabe, *Solid State Ionics* **79,** 84 (1995).
24. A. Watanabe, *J. Solid State Chem.*, **120,** 32 (1995).
25. A. Watanabe, *Solid State Ionics*, in press.
26. J. W. Visser, *J. Appl. Crystallogr.* **2,** 89 (1969).
27. D. E. Appleman and H. T. Evans, Jr., NTIS PB-216, 188 (1973).
28. A. Watanabe, unpublished data.
29. R. D. Shannon, *Acta Crystallogr. Sect. A* **32,** 751 (1976).